# Coarse-Grained Brownian Dynamics Simulations of Electrophoresis of DNA Molecules from Generalized Reptation Models

**Richard S. Graham*,† and Ronald G. Larson**

*Department of Chemical Engineering, University of Michigan, Ann Arbor, Michigan 48109*

*Received August 18, 2006; Revised Manuscript Received October 25, 2006*

ABSTRACT: We derive a course-grained Brownian dynamics simulation algorithm for the motion of DNA chains under an external electric field. We generalize a model for bulk rheological response of entangled polymers by Schieber et al. [*J. Rheol.* **2003**, *47*, 213], allowing both rheology and electrophoresis to be modeled under the same theoretical framework. The effect of the external electric field is included by modifying the strand free energy, which then influences both the monomer sliding dynamics between entanglements and the renewal of entanglements at the chain ends. We also modify the free energy to include the finite extensibility of the chain segments and account for changes in local chain mobility with chain configuration. The resulting model gives a detailed account of the chain dynamics on length scales above the tube diameter and is suitable to model a wide range of field conditions. Simulation results for a constant-field mobility are presented, which fully characterize the model under these conditions. We ensure that the model captures known scaling regimes from analytic theory and compare the predictions to a set of experimental data for constant-field mobility of double-stranded DNA in agarose gels at a range of gel concentrations. This data comparison provides a method to characterize DNA−matrix systems, providing possibilities for modeling of more general field conditions.

## 1. Introduction

Studies of the dynamics of DNA during electrophoresis provide insight into the fundamental physics of confined, highly deformed polymers and aid the development of practical tools for molecular biology. The separation of DNA is particularly important since it allows access to a range of relevant properties through the analysis of DNA fragments by size. DNA separation is frequently performed by driving the chains through an entangling medium with an external electric field. If the drift velocity under the electric field is sufficiently dependent on chain length, then fractionation results. However, separation of DNA by electrophoresis suffers from a number of practical limitations. With an electric field that is constant with time double-stranded DNA fragments of up 30−40 kilobase pairs (kbp) can be separated. However, separation of larger fragments is not possible with constant fields since the drift velocity becomes independent of chain length. A qualitatively similar loss of resolution with chain length is also encountered for single-stranded DNA. As an example, DNA sequencing, which involves fractionation of single-stranded DNA, is essential to modern molecular biology, and the need for evermore efficient and convenient sequencing methods is expected to grow as future applications are found.[1,2] Many sequencing methods require bulk amounts of DNA,[3] and although there are alternatives, requiring only a limited number of molecules, such as fluorescence in-situ hybridization (FISH), they offer poorer resolution.[4] An ideal technique would combine rapid, high-resolution sequencing from a small number of molecules. An understanding of the molecular mechanisms that control the dynamics of entangled DNA chains under electric fields may help resolve these issues.

Time-dependent electric fields have been advanced as possible solutions to some of these separation and sequencing issues. Pulsed fields, in which the field direction varies periodically in with time, can be used to separate longer DNA chains.[5,6] For example, the drift velocity depends strongly upon pulsing frequency for molecular weights extending into hundreds of kbp for double-stranded DNA. However, practical application of these techniques encounters difficulties with the speed a reliability of separation.[7] Alternatively, stretching of DNA molecules by electric fields offers possibilities for sequencing small numbers of molecules, by either selective labeling[8] or cutting[9,10] of specific nucleotides on stretched chains. Entangled DNA molecules have been successfully stretched with oscillating electric fields by Ueda and co-workers.[11−13] This technique, known as electrostretching, is particularly attractive since it may be incorporated into practical, integrated DNA analysis devices.[14,15] In each of these cases the difficulties encountered in constant-field electrophoresis are avoided because the time-dependent field never allows the chains to reach a steady state with respect to a particular field direction or magnitude. In fact, the results from both techniques suggest a resonance effect with the underlying molecular time scales. In order to elucidate and predict the physics governing these processes, which have considerable practical importance, there is a clear need for a comprehensive molecular model. Such a model must capture the DNA dynamics in entangled media subjected to external electric fields and be sufficiently general to model both constant fields and time-dependent fields.

In this paper we build upon existing approaches to the simulation of electrophoresis. We identify those issues with existing models that prevent them from satisfying the above requirements. These shortcomings are tackled by incorporating more detailed entanglement physics, drawing upon insights gained from molecular modeling for bulk flows of entangled polymer fluids. From a slip-link description of the entangling medium, we derive a single chain, coarse-grained Brownian dynamics algorithm for entangled DNA molecules that can model a wide range of external field conditions. We quantitatively test this model against constant-field DNA mobility. From

* Corresponding author. E-mail: r.s.graham@leeds.ac.uk.
† Current address: Polymers and Complex Fluids Group, School of Physics and Astronomy, University of Leeds, Leeds LS2 9JT, United Kingdom.

10.1021/ma061912+ CCC: $37.00 
Published on Web 12/15/2006

this comparison we are able to extract molecular parameters for the DNA−matrix system which will be useful when modeling time-dependent fields.

## 2. Modeling of Entangled Systems

In electrophoresis experiments the interactions between distinct DNA molecules are unimportant. The chain dynamics are dominated by the interactions between a single DNA chain and the surrounding medium, which suggests that single molecule simulations are a natural theoretical tool with which to approach this problem. Indeed, a number of computation investigations of electrophoresis in which the entanglement environment is modeled by a series of fixed obstacles have been made.[16−18] While many significant insights have been gained from simulations involving this direct representation of the gel constraints, the approach has two limitations. Significant computational time is required to resolve the chain motion on short length scales, which wastes computational resources since these small-scale configurations often remain in equilibrium. Additionally, these models require numerous parameters to describe the entangling medium, and the connection between these parameters and experimental conditions is ambiguous. In contrast, the Doi and Edwards tube model[19] offers a minimal parameter representation of the entangling environment. The model asserts that, since one chain may not pass through another, each chain experiences strongly restricted motion lateral to its curvilinear path but no confinement for motion parallel to it. The constraints are assumed to be felt only beyond a length scale, *a*, the single parameter that characters the environment. Effectively, each chain is confined to a tube of diameter *a*. The chain ends are able to explore the mesh free of this topological constraint, which allows the chain to renew its configuration. In the case of rheological modeling, extensive quantitative comparisons with tube model predictions have been made (see refs 20−22 for a recent summary). Furthermore, analytic tube-based theories have successfully explained a number of scaling relations seen in steady-field electrophoresis.[23−25] A bead and spring type Brownian dynamics simulation algorithm for electrophoresis was developed by Noolandi et al.,[26] which was based on a generalized tube model. However, Brownian dynamics simulations of entangled chains for rheological modeling have advanced significantly since this work. In addition, the connection between DNA dynamics under electrophoresis and rheology has been further strengthened by recent direct bulk rheological measurements on DNA fluids, in both the dilute[27,28] and entangled[29] regimes. Thus, we look to adapt modern coarse-grained simulation algorithms, originally developed to model rheological measurements, to produce a general molecular model for electrophoresis.

**2.1. Temporary Network-Type Models and Electrophoresis.** Rheological measurements on entangled polymer fluids underpin much of the theoretical understanding of these fluids. Early rheological models for polymer fluids adapted the network theory of rubber elasticity, adding dissipative relaxation through phenomenological postulation of the rates of creation and destruction of the network junctions. Recently, this temporary network approach has been refined to produce a number of algorithms for coarse-grained simulation of entangled polymer fluids.[30−32] These models have two significant departures from traditional temporary network models. The number of monomers in an entangled strand is not a constant parameter but fluctuates according to some dynamics, which are specified by molecular theory. Thus, the monomers are allowed to slide through the network junctions, which eventually permits long-range sliding motion, known as reptation. Furthermore, the dynamics resulting from this monomer motion trigger the creation and destruction of entanglement junctions or slip-links, in place of the earlier phenomenological approach. Thus, the restriction of chains' lateral motion, which is characteristic of the tube model, is enforced through the entanglement junctions, and these junctions are renewed as the chain ends explore new regions of the melt. These approaches have been used to model the dynamics of entangled chains under both linear and nonlinear deformations.

The temporary network approach has also been applied to electrophoresis modeling by Zimm,[33,34] in the so-called lakes−strait model. In this model the entanglement environment is pictured as a heterogeneous mesh, comprising open spaces and tight pores. Chains can move freely in the spaces between gel fibers, termed lakes, yet are strongly confined in the tight pores or straits. An entangled DNA chain occupies a series of lakes which are joined by short, narrow gateways or straits, in which the chain is tightly confined. In terms of the more recent rheological models, the lakes play the same role as entanglement segments, and the straits are equivalent to entanglement junctions. It is worth noting that Zimm's work substantially predates the recent applications to rheology, and although the lakes−straits picture of entanglements is somewhat nonstandard when compared to current ideas, Zimm's simulation algorithm is remarkably similar the modern implementations discussed above. The lakes−straits model successfully predicted the antiresonance effect in pulsed field electrophoresis. Experimentally, if a periodically varying electric field is superimposed over a constant field, then the mobility vs pulsing frequency for a fixed molecular weight will contain a deep minimum.[5] The lakes−straits model mirrored these results. The simulation results also allowed the tube-based approach to make contact with the emerging results for direct molecular visualization of electrophoresis.

While the lakes−straits model was a significant advance, there were a number of limitations in its implementation. These either arise from the algorithm itself or are due to the limitations of computing power at the time the model was developed. Some of these issues are general to the temporary network approach, and some guidance on addressing these can be found in the more recent rheological models. The computational problems can be addressed through a combination of refined numerical techniques and recent advances in computational power. Finally, we may modify the physical assumptions of the model where necessary. The lakes−straits heterogeneous picture of the entanglement environment is at odds with current ideas about the nature of entanglements in fluids of flexible polymers, such as polyacrylamide. Neutron and X-ray scattering data show no significant correlations in density fluctuations in concentrated polymer fluids.[35] Furthermore, some recent theories argue that entanglements are due to the net effect of many delocalized fluctuating interactions between multiple neighboring chains, and so a homogeneous, mean-field picture of the entanglement effect is closer to the correct physics.[36,20] Even though slip-link-based models generally assume that entanglements consist of predominantly two-chain interactions,[30,32,37] they are still based on a homogeneous picture of the entanglement environment. Agarose gels are somewhat different due to the rigidity of the constituent fibers which cause heterogeneity in the gel pore size. Nevertheless, mean-field approaches to the confining potential appear to be able to describe DNA mobility in such gels.[40] This may be because a long DNA chain will simultaneously occupy many gel pores or because, during a long electrophoresis run, a DNA chain samples a very large number of gels pores. For these reasons a mean-field approximation for

the effective confining potential appears to work. It is, therefore, convenient to re-formulate any part of the lakes−straits model that relies upon the assumption of inhomogeneity of the entangling medium. For example, in the lakes−straits algorithm, the electric force is only imposed on chain segments in the straits, while those in the lakes are ignored. In our approach, the effect of the field on all segments of the chain will be accounted for.

Renewal of entanglements at the chain ends can be problematic in Brownian dynamic simulations of entangled polymers. Intuitively, one would like to implement the idea that as the chain drains from the end segment, eventually that segment should be destroyed since it is no longer occupied; conversely, as monomers accumulate in the end segment, eventually a new segment should be made. The simplest implementation of this idea into a simulation algorithm involves minimum and maximum threshold values for the occupancy of the end segments. Entanglement segments are created or destroyed when the appropriate condition is violated. This approach has been used in rheological modeling[30] and was also used in the Noolandi et al. electrophoresis model,[26] where the influence of the external field on the orientation of newly placed segments was also ignored. Unfortunately, this simple approach spoils the time-step convergence of the simulation algorithm. As the time step is decreased, the simulation resolves increasingly fine Brownian fluctuations of the chain ends, resulting in evermore frequent creation and destruction events. Since the motion of the chain ends controls renewal of tube segments, and ultimately the chain configuration, a detailed account of this renewal process is desirable and could be especially important for strong time-dependent fields. In the lakes−straits model the rate of overflow of the chain ends was derived on the basis of diffusion of the dangling ends over a potential barrier, resulting in a probability per unit time of entanglement renewal. However, this derivation explicitly relies upon the lakes−straits inhomogeneous picture of the entanglement environment, and we would like to rectify this to be consistent with a mean-field picture of entanglements. Furthermore, it was argued that the influence of an external electric field on entanglement creation is negligible in electrophoresis and that Boltzmann weighting of the orientation of the new segments in the external field is more than sufficient.[33] While this may be true for low fields, we believe that biasing of newly created segments by the field is essential to quantitative modeling of general time-dependent fields.

This end renewal question also arises in rheological modeling; consequently, some alternative strategies can be found in these models. Masubuchi et al.[30] used a simple threshold condition, similar to the approach that we discounted above. The problem of time-step convergence is bypassed by enforcing a fixed time interval between each application of the condition, regardless of the simulation time step. The chosen time interval is the Rouse time of an entanglement segment, $\tau_e$, which is the fastest resolved time scale in these models. Similarly to the lakes−straits model, Schieber et al.[32] also derived a probabilistic test for entanglement renewal. They used a detailed balance argument to derive expressions for the probability per unit time for both creation and destruction of entanglements, tacitly assuming a homogeneous picture of the entanglement environment. The resulting algorithm is stable to changes in the time step and is controlled by the free energy of the chain, thus providing a framework that can naturally be extended to electrophoresis modeling. See section 3.3.2 for more details of this process.

All temporary network-type models have a degree of inherent numerical stiffness since, even if the chain spring constant is Gaussian, the number of monomers in an internal strand cannot fall below zero. This condition is enforced by a singularity in the strand free energy as the number of strand monomers shrinks to zero. This significantly complicates numerical solution of the model. Masubuchi et al.[30] tackled this problem by imposing an artificial minimum value on the number of monomers in each segment, which was set close to zero, and then demonstrating that their results were not sensitive to the precise value of this cutoff. However, this is unlikely to be true for situations involving a significant chain stretching. Similarly, the lakes−straits model imposes a crude form of finite extensibility on the each segment by locking the number of monomers in each segment once it reaches some minimum value, allowing sliding but no further stretching. In the most complete treatment, Schieber et al.[32] use an implicit time stepping scheme. This scheme ensures that singularities in the chain free energy cannot be passed over so the numbers of monomers in each entanglement segment remains within the bounds of physically meaningful values. Although Schieber et al. used a Gaussian form for the strand free energy, we will generalize their approach to model finitely extensible chains.

Zimm's direct simulation of the lakes−straits model[33] involved a number of numerical shortcuts to reduce the computational effort required to solve the model, at the cost of less accurate solutions. The Brownian forces were implemented only at the chain ends to ease the numerical disruption caused by Brownian jostling of the monomers in internal segments. This is effectively a neglect of diffusion-driven fluctuations in the tube contour length, yet the biased reptation theory with fluctuations (BRF) demonstrated that fluctuations play an essential role in the quantitative modeling of constant-field electrophoresis.[24,38] Similarly, we expect these fluctuations to have a quantitative effect on more general time-dependent fields. For example, Ueda et al.[12] proposed a mechanism for electrostretching in which hairpin configurations of the chain play a key role. Internal chain fluctuations and the selection of new entanglement segments will strongly affect the formation of these hairpins and the response of the chain when in this configuration. In a further approximation, Zimm used a crude implementation of finite chain extensibility as discussed above. Recent advances in computing power mean that neither numerical shortcut is now necessary, and we are able to study the full effect of Brownian fluctuations on the internal modes of a chain and can smoothly introduce chain finite extensibility through the appropriate strand free energy.

Many of the above elements have been incorporated into a nonlocal Monte Carlo simulation algorithm by Duke and Viovy,[39] which describes DNA electrophoresis behavior well.[40,41] However, there are a number of important differences in the work presented here. We use a Langevin stochastic formulation, which although based on similar physics to the nonlocal Monte Carlo approach, provides a significantly different description of the chain dynamics. Our model allows a continuous description of the monomer sliding dynamics, which is controlled by a well-defined force law for the chain extension. Our model also contains a detailed description of the influence of the electric field on the creation of new entanglements at the chain ends. In this algorithm the orientation, length, and number of monomers in a newly created segment are selected stochastically from a distribution determined by the chain free energy, therefore accounting for thermal fluctuations, the external field, and finite extensibility of the chain segments.

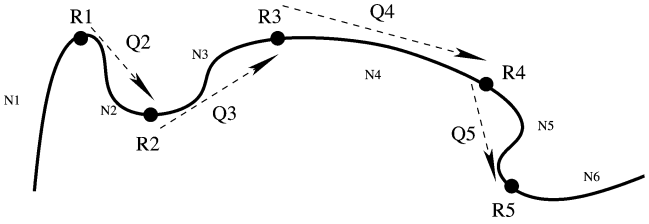


**Figure 1.** Coarse-grained representation of an entangled polymer chain, indicating the degrees of freedom used in this model.

## 3. The Schieber et al. Temporary Network Model

As discussed above, the simulation algorithm of Schieber et al.[32] has a number of advantages over other models when we consider generalizations to electrophoresis modeling. Specifically, the approach can readily include the effects of chain finite extensibility and an external electric field, and the model naturally allows a detailed consideration of the influence of the external field on the entanglement creation dynamics. Before generalizing the model, we present a brief review of the rheological approach, for which full details of the derivation may be found in refs 32 and 42.

**3.1. Chain Description.** The test chain is coarse-grained on the length scale of the entanglement network. It comprises $N_K$ Kuhn steps or "monomers'' of step length $b$ and is divided into $Z$ strands, which join together $Z - 1$ entanglement junctions (see Figure 1). The chain configuration is fully specified, up to the chosen level of coarse-graining, by the position of each entanglement junction, along with the number of monomers in each strand. The two end segments, $N_1$ and $N_z$, are attached to a single entanglement junction and are referred to as dangling ends. Thus, the degrees of freedom in the model are $\{\mathbf{R}_i\}$, the position vectors of the entanglement junctions, and $\{N_i\}$, the number of monomers between junctions $i - 1$ and $i$. All chain configurations on shorter length scale are assumed to be in thermal equilibrium. The total number of entanglement strands varies with time, fluctuating according to the dynamics of the chain, with the total number of monomers fixed. Also shown in Figure 1 are the vectors joining consecutive entanglement junctions, $\mathbf{Q}_i = \mathbf{R}_i - \mathbf{R}_{i-1}$, which we will refer to throughout this paper. A version of the model was derived in which the number of monomers occupying an entanglement strand is taken to be a continuous variable.[32] We adopt this continuous approach throughout this paper.

**3.2. Chain Free Energy.** The chain free energy governs both the equilibrium properties and the dynamics of the chain ensemble. For the free energy of an internal strand, $F_s$, Schieber et al.[32] used the standard expression for a Gaussian random walk

$$\frac{F_s(\mathbf{Q}_s,N_s)}{k_BT} = \frac{3Q^2}{2N_sb^2} + \frac{3}{2}\ln\left(\frac{2\pi N_sb^2}{3}\right) + \ln N_e \qquad (1)$$

where the subscripts s denotes an internal strand and $N_e$ is the average equilibrium number of Kuhn steps, or "monomers'', per entanglement strand. The ln $N_e$ term is a modification to the usual Gaussian free energy. It accounts for the free energy cost per entanglement segment and ensures the chain has the appropriate average number of entanglements in equilibrium $\langle Z^{eq}\rangle = N/N_e$. For the free energy of a dangling end, $F_E$, Schieber et al.[32] used the following form

$$\frac{F_E(N_E)}{k_BT} = -\frac{1}{2}\ln N_E + \ln N_e \qquad (2)$$

where the subscript E denotes an end strand. Later we will modify both of these free energies to incorporate finite chain extensibility and an external electric field in order to adapt the theory to electrophoresis modeling.

The chain equilibrium distribution is given by the Boltzmann factor of the total free energy along with the constraint that the total number of monomers must be $N_K$

$$p^{eq}(\{Q_i\},\{N_i\}) = \frac{1}{J}\exp[-(\sum_{i=2}^{Z-1}F_s(\mathbf{Q}_i,N_i) + F_E(N_1) + F_E(N_Z))/k_BT]\delta(N_K - \sum_{i=1}^{Z}N_i) \qquad (3)$$

where the delta function enforces the monomer constraint and $J$ normalizes the distribution. From this expression Schieber et al.[32] derived an algorithm for generating chains with this equilibrium distribution.

**3.3. Chain Dynamics.** The dynamics describing the exchange of monomers between segments in the model are described by a Fokker−Planck equation for the probability density function for the chain configuration, $p(\{\mathbf{Q}_i\},\{N_i\})$

$$\frac{\partial p}{\partial t} = \sum_{ij}\frac{\partial}{\partial N_i}L_{ij}\left[\left(\frac{\partial F}{\partial N_j}\right)_{T,\{\mathbf{Q}i\}}p + k_BT\frac{\partial p}{\partial N_j}\right] \qquad (4)$$

where $L_{ij}$ is the mobility matrix, defined in eq 6. The monomers diffuse in response to Brownian forces and are driven across the entanglement junctions by differences in the chemical potential

$$\mu_i = \left(\frac{\partial F}{\partial N_j}\right)_{T,\{\mathbf{Q}i\}} \qquad (5)$$

which originate from the spring force and, in our modification, the external electric field.

**3.3.1. Mobility Matrix.** Equation 4 requires us to stipulate the mobility matrix $L_{ij}$, which specifies the rate of the response of the system to an external force. This external force is expressed as a difference in chemical potential between two neighboring segments. Differences in chemical potential cause monomers to leave one segment and enter its neighbor by sliding across the junction point. This results in the following form of the mobility matrix as used by Schieber et al.[32]

$$L_{ij} = \frac{1}{k_BT\tau_K}\begin{cases}2 & i = j\\ -1 & i = j \pm 1\\ 0 & \text{otherwise}\end{cases} \qquad (6)$$

This matrix is similar to that from the Rouse model. The tridiagonal property of $L_{ij}$ enforces the correct chain connectivity, the condition $\sum_i L_{ij} = 0 \forall j$ ensures monomer conservation, and the rate of monomer sliding is set by the time scale $\tau_K = \zeta b^2/k_BT$, where $\zeta$ is the friction coefficient per monomer. This quantity leads to the Rouse time of an entanglement segment, $\tau_e = N_e^2\tau_K$, which is the fastest time scale that is resolved by this level of coarse-graining. Schieber et al.[32] took these time scales to be constant by assuming that the mobility matrix does not change with the chain configuration. They acknowledged that this causes the total chain friction to be proportional to the fluctuating value of $Z$ and briefly discussed other possible assumptions for $L_{ij}$. Below we will derive an expression for the mobility matrix in which it fluctuates with the local chain configuration, under the assumption that each monomer carries

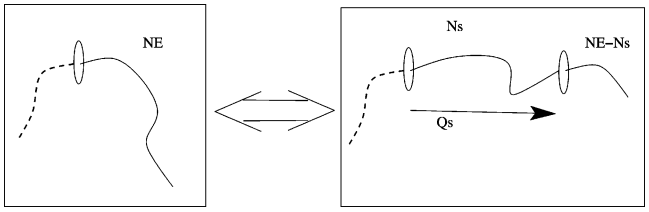


**Figure 2.** Creation of a new entanglement segment.

an equal amount of drag. The rate of this sliding process turns out to be crucial to electrophoresis modeling.

With the mobility matrix specified, eq 4 can be converted to an equivalent system of stochastic differential equations which are suitable for solution by Brownian dynamics simulation. Essentially, one must follow the general algorithm for this procedure, as described in ref 43, which leads to

$$dN_i = \frac{1}{k_B T \tau_K}(\mu_{i+1} - 2\mu_i + \mu_{i-1})\, dt + \sqrt{\frac{2dt}{\tau_K}}(dW_{i-1} - dW_i) \quad (7)$$

where $dW_i$ is a Wiener increment with zero mean and unit variance. The equations can be solved implicitly over a finite time step $\Delta t$ which ensures that the monomer occupation number remains positive.

**3.3.2. Entanglement Renewal at the Chain Ends.** Equation 4 describes the motion of monomers within the entanglement segments but does not allow for renewal of entanglement junctions at the chain ends. The probability per unit time (or rate) of creation or destruction of an end junction depends upon the instantaneous number of monomers in the corresponding end segment and is tested at each time step of the simulation. Figure 2 shows an entanglement creation event along with all relevant variables. The creation process is governed by the function $W^c(c(N_E,\mathbf{Q}_s,N_s)$, which denotes the probability per unit time of creating a new segment of vector $\mathbf{Q}_s$ with $N_s$ monomers from a dangling end of $N_E$ monomers. Expressions for this "test creation event'' are obtained by asserting a form for the destruction probability, $w^d(N_E)$; then the following detailed balance condition provides the joint creation probability per unit time, $W^c(N_E,\mathbf{Q}_s,N_s)$:

$$W^c(N_E,\mathbf{Q}_s,N_s) = \exp\left[\frac{F_E(N_E) - F_s(\mathbf{Q}_s,N_s) - F_E(N_E - N_s)}{k_B T}\right] w^d(N_E - N_s) \quad (8)$$

where $W$ denotes a joint probability density and $w$ denotes a marginal probability density. Note the slight misprint in the corresponding equation from ref 32 which is corrected here. Once the following form for the destruction probability per unit time is asserted

$$w^d(N_E) = \frac{N_e}{\tau_e}\sqrt{\frac{3}{N_E}} \quad (9)$$

then progressively integrating the joint probability (eq 8) leads to an explicit expression for $w^c(N_E)$ along with the conditional probability distributions, from which the properties of the newly created entanglement segment can be generated (see section 4.2 for details of this derivation). The form of eq 9 ensures that the number of monomers in the new segment $N_s$ is chosen evenly between $0...N_E$, which is consistent with the assumption of a homogeneous distribution of potential entanglement points. It is also the simplest function that leads to the logical properties:

$$\lim_{N_E\to 0} w^c(N_E) = 0 \qquad \lim_{N_E\to\infty} w^c(N_E) = \infty$$
$$\lim_{N_E\to 0} w^d(N_E) = \infty \qquad \lim_{N_E\to\infty} w^d(N_E) = 0 \quad (10)$$

Underlying this derivation is the assumption that the dangling ends have sufficient time to fully explore the majority of microstates available to them and that potential sites for the creation of an entanglement junction are evenly distributed throughout the space explored by the dangling end. Therefore, the probability of creating a new entanglement junction at any position is proportional to the probability of finding a monomer from the dangling end in close vicinity.

It is interesting to note that eq 9, as postulated in ref 32, cannot be written in a universal form that depends only on $N_E/N_e$ and not $N_e$ itself. Consequently, both the creation and destruction probability functions have an explicit dependence on $N_e$. This nonuniversality in the prefactor of this function is quite contrary to usual models of polymer dynamics. In section 4.2.1 we make a simple modification of this prefactor to a universal form in our formulation of the model, and in section 5 we show that the nonuniversal form artificially overpredicts the influence of contour length fluctuations on moderately entangled chains.

In this paper we adopt the general formalism of Schieber et al.[32] but change both the chain free energy and mobility matrix in order to make the model suitable for simulations of electrophoresis.

## 4. Electrophoresis Model

In this section we present a new simulation algorithm for electrophoresis modeling which is built upon the rheological model of Schieber et al.[32]

**4.1. Modified Free Energy.** In order to generalize the temporary network model to electrophoresis, we need to include the effect of an external electric field. Furthermore, since we wish to model highly extended chains, we must also account for changes in the strand force−extension law as the strand approaches full extension. These two effects can be entirely incorporated into the strand free energy, and from this they influence both the monomer sliding dynamics and entanglement renewal.

Taking the effective charge per monomer to be $\xi q$ where $\xi$ is a dimensionless parameter that characterizes the degree of counterion screening, then a field of magnitude $E$ acting along the $x$-axis results in a potential of $\Psi(x) = q\xi Ex$. We assume that the average position of each monomer is the center of its respective segment (see Figure 3), which is consistent with the coarse-graining of the model, to obtain the following expression for the field contribution to the free energy

$$F_s^{field} = -q\xi E\left(R_x^{s-1} + \frac{1}{2}Q_s\cos\theta\right)N_s \quad (11)$$

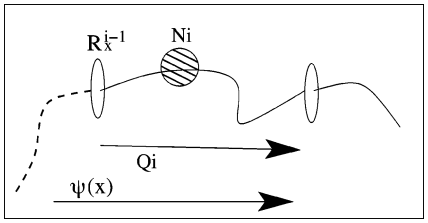


**Figure 3.** Computing the charged segment potential.

where $\theta$ is the angle between $\mathbf{Q}_s$ and the field direction. For the chain ends, the segments are assumed, on average, to be positioned at the end entanglement point

$$F_E^{field} = -q\xi E R_x^E N_E \tag{12}$$

Although these free energies depend upon the absolute position of the previous entanglement point, we will always be comparing the difference of two free energies, and this difference can be expressed entirely in terms of the segment orientations, $\{\mathbf{Q}_s\}$.

To model highly extended chains, we note that the minimum number of Kuhn steps required to span an internal segment of length $Q_s$ is

$$N_s^{min} b = Q_s \tag{13}$$

and the free energy must account for the significant loss of chain entropy as the strand approaches this configuration. The appropriate, finitely extensible free energy can be expressed in terms of the inverse Langevin function.[44] We use the form suggested by ref 32, which is obtained by integrating Cohen's Padé approximant of the inverse Langevin function[45]

$$\frac{F_s^{spring}}{k_B T} = \frac{Q_s^2}{2N_s b^2} - N_s \ln\left[1 - \left(\frac{Q_s}{bN_s}\right)^2\right] + \frac{3}{2}\ln\left[\frac{2\pi N_s b^2}{3}\right] + \ln N_e \tag{14}$$

Note that this form of the free energy diverges as $N_s \rightarrow N_s^{min}$, as required. An alternative choice to incorporate finite extensibility would be to use the wormlike chain model to account for chain semiflexibility in the model. However, Hur et al.[46] performed Brownian dynamics simulations under shear flow for both inverse Langevin-type chains (similar to eq 14) and wormlike chains and demonstrated that there was very little difference in the stretching dynamics between the two chain types. Thus, there is no reason to expect much difference would result from using a different finitely extendable spring. Alternative spring laws could, however, be incorporated into algorithm, if required.

The free energy of the dangling ends is not affected by the finite extensibility condition. Our final expression for the free energy of an internal segment is thus

$$\frac{F_s}{k_B T} = \frac{Q_s^2}{2N_s b^2} - N_s \ln\left[1 - \left(\frac{Q_s}{bN_s}\right)^2\right] + \frac{3}{2}\ln\left[\frac{2\pi N_s b^2}{3}\right] + \ln N_e - q\xi E\left(R_x^{s-1} + \frac{1}{2}Q_s \cos\theta\right)N_s \tag{15}$$

**4.2. Entanglement Creation Dynamics.** We discussed in section 2 the influence of entanglement renewal at the chain ends on the chain dynamics under an electric field. Thus, it is important to derive an unambiguous procedure to describe this process. In section 3.3.2 we described the approach to entanglement renewal used by Schieber et al.[32] to model the Gaussian zero-field case. This approach can be directly applied to our modified free energy, resulting in an algorithm that captures the influence of the external electric field on both the frequency of creation events and the orientation of newly created segments. The underlying approach is the same; however, the inclusion of the field significantly increases the complexity of the integration and the resulting probability density functions. As before, we substitute the desired free energy expression into the detailed balance eq 8 to obtain a master joint probability function. This function can be split into the following subprobabilities

$$W^c(\mathbf{Q}_s, N_s, N_E) = p(\mathbf{Q}_s|N_s, N_E)\, p(N_s|N_E)\, w^c(N_E) \tag{16}$$

where $N_E$ is the number of segments in the current dangling end and $N_s$ and $\mathbf{Q}_s$ are the number of monomers and segment vector, respectively, for the newly created segment (see Figure 2). The single-variable marginal distribution distribution, $w^c(N_E)$, is found by integrating over all allowed values of $\mathbf{Q}_s$ and $N_s$; the conditional probability $p(N_s|N_E)$ is found from

$$p(N_s|N_E) = \frac{p(N_s, N_E)}{w^c(N_E)} \tag{17}$$

and similarly for $p(\mathbf{Q}_s|N_s)$. In the simulation algorithm the creation probability per unit time, $w^c(N_E)$, is tested, for both chains ends, at each time step. Whenever the test is positive, a new segment is generated with properties drawn from the derived conditional probabilities.

In this work we do not consider the effect of chains leaking laterally between the tube constraints, known as hernia formation. We do not expect this process to have a significant effect on steady-field mobility or on electrostretching since the formation of hernias in a fully stretched chain will be very unlikely due to the entropy cost of further extending the chain. We note that Zimm argued that this mechanism is needed to predict a sufficiently deep antiresonance effect to match that seen in pulsed field electrophoresis experiments,[33] as was recently confirmed by ref 47. The detailed balanced based procedure for renewal of entanglement junctions at the chain ends, as outlined above, could naturally be generalized to self-consistently model hernia formation, but we leave this to future work.

**4.2.1. Modified Entanglement Destruction Probability.** As noted in section 3.3.2, the form of the entanglement destruction probability used in ref 32 has an explicit dependence on $N_e$, rather than depending only on the universal ratio of $N_E/N_e$. In our simulations we modify the prefactor of eq 9 to obtain a universal expression. Thus, the destruction probability becomes

$$w^d(N_E) = \frac{1}{\tau_e}\sqrt{\frac{3N_e}{N_E}} \tag{18}$$

Note the factor of $\sqrt{N_e}$ difference with eq 9. In section 5 we demonstrate that the nonuniversal form artificially overestimates the influence of contour length fluctuations in moderately entangled chains, whereas the universal form of eq 18 produces low field behavior that is in significantly better agreement with scaling theories and experimental data for constant-field mobility. This improved form for $w^d(N_E)$ can now be carried over into rheological modeling, which illustrates how using the same

framework for both electrophoresis and rheology may lead to improvements for both.

**4.2.2. Dimensionless Units.** We introduce the following dimensionless units for length, monomer number, electric field, time, and number of entanglements

$$\tilde{Q} = \left(\frac{Q}{\sqrt{N_e}b}\right), \quad \tilde{N} = \frac{N}{N_e}, \quad \epsilon = \frac{q\xi N_e^{3/2} b}{k_B T} E, \quad Z = \frac{N_{bp}}{N_e N_K^{bp}}, \quad \tilde{t} = \frac{t}{\tau_e} \tag{19}$$

where $N_{bp}$ is the number of DNA base pairs per chain, $N_K^{bp}$ is the number of base pairs per Kuhn step, and $\tau_e$ is the Rouse time of an entanglement segment, the relaxation time of a chain that is just long enough to span a single entanglement segment ($\tau_e = N_e^2 b^2 \zeta / k_B T$). From these quantities a useful reference value for the electrophoretic mobility can be obtained. In the limit of short chains, the entangling matrix has no effect, and the chains are in the free draining limit. In this case the electrophoretic mobility is independent of molecular weight and is given by the effective charge per Kuhn step divided by the drag per Kuhn step. In terms of our parameters this is given by

$$\mu_0^E = \frac{q\xi}{\zeta} \tag{20}$$

This quantity should not be confused with the free solution mobility, the chain mobility in the absence of an entangling matrix. Differences between these two quantities are to be expected since the monomer drag, $\zeta$, may vary somewhat with matrix concentration.

**4.3. Electrophoresis Simulation Algorithm.** First, an equilibrated chain is obtained by generating a chain from the probability distribution given by eq 3, following the method of Schieber et al.,[32] using the chain free energy with no electric field. The simulation time is then advanced in small time increments with two stages to each time step, sliding dynamics, and entanglement creation/destruction.

The monomer sliding stage is governed by a Langevin equation, which controls the sliding rate from each entanglement segment $N_i$. In dimensionless units this is

$$d\tilde{N}_i = d\tilde{t}(\tilde{J}_{i,i-1}(\tilde{\mu}_{i-1} - \tilde{\mu}_i) + \tilde{J}_{i,i+1}(\tilde{\mu}_{i+1} - \tilde{\mu}_i)) + \sqrt{2d\tilde{t}}(\sqrt{\tilde{J}_{i,i-1}}dW_{i-1} - \sqrt{\tilde{J}_{i,i+1}}dW_i) \tag{21}$$

where $\tilde{J}_{i,i-1} = 2(\tilde{N}_i + \tilde{N}_{i-1})/(\tilde{Q}_i + \tilde{Q}_{i-1})^2$ is the dimensionless mobility matrix, $\tilde{\mu}_i = (N_e/k_B T)(\partial F/\partial N_i)$ is the dimensionless chemical potential, and the $dW_i$ are a set of independent Wiener increments of unit width. The sliding step is performed by numerically solving the system of equations defined by eq 21 implicitly over a short finite time interval $\Delta\tilde{t}$, for $i = 1...Z$. For details of the derivation of eq 21 and the numerical algorithm for this stage see Appendix A.

For the entanglement creation and destruction stage we first test for the destruction of entanglements at both chain ends. The probability of removing the end entanglement is given by

$$w^d(\tilde{N}_E) = \Delta\tilde{t}\sqrt{\frac{3}{\tilde{N}_E}} \tag{22}$$

where $\tilde{N}_E$ denotes the dimensionless number of monomers in the dangling end. Then we test for the creation of a segment.

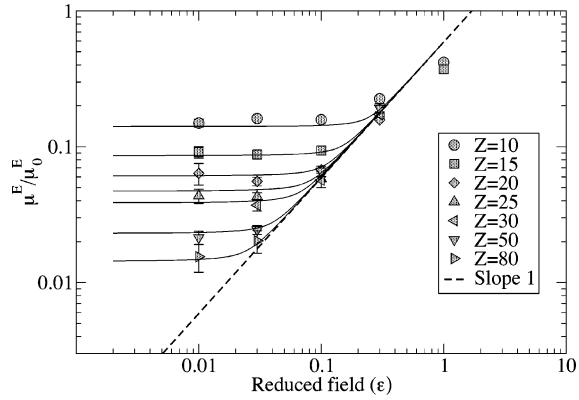


**Figure 4.** Simulation results for constant-field mobility vs field for a range of molecular weights. The solid lines are the results of the interpolation function, eq 27.

The overall creation process is governed by the joint probability density

$$W^c(\tilde{N}_E, \tilde{\mathbf{Q}}_s, \tilde{N}_s) = \Delta\tilde{t}\sqrt{\frac{3}{(\tilde{N}_E - \tilde{N}_s)}} \exp[\tilde{F}_E(\tilde{N}_E) - \tilde{F}_s(\tilde{\mathbf{Q}}_s, \tilde{N}_s) - \tilde{F}_E(\tilde{N}_E - \tilde{N}_s)] \tag{23}$$

where $\tilde{F}$ is the strand free energy (over $k_B T$) and $\tilde{N}_s$ and $\mathbf{Q}_s$ are the number of monomers on length of the newly created segment, respectively. The required marginal and conditional probabilities are obtained by successive integration of eq 23. This general method is independent of the free energy expression, although the integration strategy depends on the functional form of the free energy. Expressions for the free energies in the presence of a field are given in eqs 15, 2, and 12, and Appendix B contains our integration method for Gaussian and finitely extensible chains.

## 5. Results

The constant-field electrophoretic mobility, $\mu^E$, is defined as

$$\mu^E = \frac{v_{drift}}{E} \tag{24}$$

where $v_{drift}$ is the chain drift velocity under a constant electric field. We use our simulation algorithm to compute the mobility by obtaining a drift velocity from an average over a long simulation run. Our results provide the quantity

$$\mu^E_{simulation} = \frac{\tilde{v}_{drift}}{\epsilon} = \frac{v_{drift}}{E}\frac{\tau_e}{\sqrt{N_e}b}\frac{k_B T}{q\xi N_e^{3/2} b} \tag{25}$$

which, from the definition of the dimensionless units (section 4.2.2), shows that $\mu^E_{simulation} = \mu^E/\mu_0^E$. For all results in this section a value of $N_e = 100$ was taken for the finite extensibility parameter (see eq 14); however, identical results were obtained using the Gaussian form of the strand free energy, indicating that the influence of finite extensibility on constant field mobility is small.

A number of asymptotic results for the constant-field mobility, which have been observed in experiments for both double and single stranded DNA,[40,48,49] can be explained by the BRF model.[24,50] Our simulation algorithm recovers these scaling results and also models the crossover regimes between these behaviors. Figure 4 shows the variation of mobility with field strength for a range of molecular weights. All error bars represent the statistical uncertainties, which are estimated by

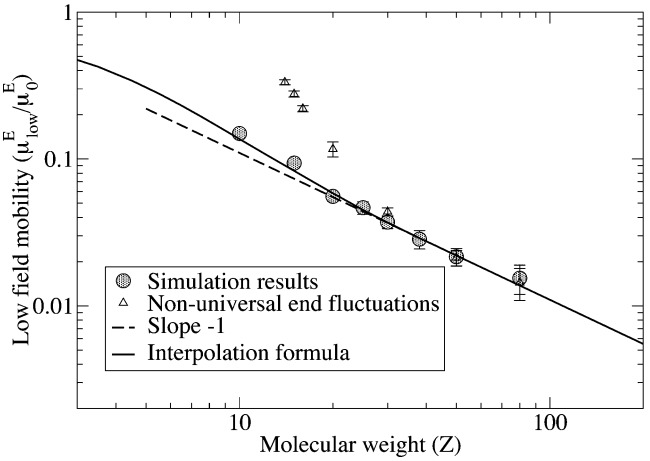


**Figure 5.** Simulation results for low field mobility vs molecular weight. The solid line is the interpolation formula of eq 26.

dividing the simulation run into a number of equal-length-long subruns and computing the standard error in the mean of this set of runs. The results are independent of the size of the subruns provided each subrun is sufficiently large. Consistent with the BRF model and experiments, two scaling regimes are evident in the simulation results. At low fields ($Z\epsilon \ll 1$) the mobility saturates to a value that is independent of applied field, $\mu^E_{low}$. In the opposite limit ($Z\epsilon \gg 1$, $\epsilon < 1$), the mobility scales linearly with the field strength and is independent of molecular weight. The simulations predict a smooth crossover between these two cases.

It is instructive to examine the variation of the low field limit of mobility ($\mu^E_{low}$) with molecular weight, which is plotted in Figure 5. The BFM model predicts that $\mu^E_{low} \sim 1/Z$ for long chains, and this behavior is produced by our simulations. There is some mild deviation from this scaling for weakly entangled chains ($Z \sim 10$), but this is to be expected since for marginally entangled chains the mobility should tend toward the free chain case (i.e., $\mu^E_{low} \to \mu^E_0$). Also shown in Figure 5 are the results obtained using the nonuniversal expression for the end entanglement segment creation and destruction probabilities (eq 9) with a value of $N_e = 100$ chosen, as suggested as a typical value by Schieber et al.[32] See section 3.3.2 for a discussion of this nonuniversal form. This form for the entanglement renewal probabilities causes significantly more frequent replacement of end segments. For moderately entangled chains this clearly overestimates the influence of contour-length fluctuations since the results show a sharp departure from the $\sim 1/Z$ scaling at around $Z = 20$, which speeds the tendency of the mobility to approach $\mu^E_0$ as $Z \to 0$. The results for long chains do not appear to be affected since the two expressions give the same values, suggesting that, in this case, the deeper contour-length fluctuations are controlled by the free energy of the internal segments.

**5.1. Interpolation Formulas.** With the asymptotic behavior of the simulations established it is convenient to describe all constant-field mobility results with a formula that interpolates between these asymptotes. For $\mu^E_{low}(Z)$ the asymptotes are $\mu^E_{low}(Z) \to \mu^E_0$ as $Z \to 0$ and $\mu^E_{low}(Z) \approx 1.1/Z$ for $Z \gg 1$, with the prefactor of 1.1 obtained by fitting simulation results for $Z \gtrsim 20$ (see the dashed line in Figure 5). These asymptotes are captured by the following equation for $\tilde{\mu}^E_{low} = \mu^E_{low}/\mu^E_0$

$$\tilde{\mu}^E_{low} = \exp(-0.27Z) + \frac{1.1}{Z}(1 - \exp(-0.01Z^2)) \quad (26)$$

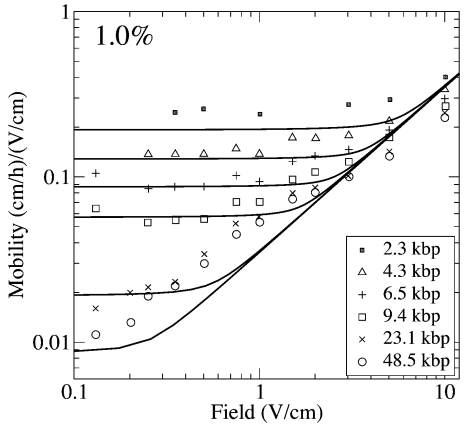


**Figure 6.** Comparison of experimental data for constant-field electrophoresis of double-stranded DNA in a 1% agarose gel by Heller et al.[40] with the interpolation formula (eq 27).

where the numerical prefactors were obtained by fitting our simulation results.

For the more general case of $\mu^E(\epsilon,Z)$, the results tend to $\mu^E_{low}(Z)$ at low fields and $\mu^E/\mu^E_0 \approx 0.67\epsilon$ when $Z\epsilon$ is large, where the value of 0.67 is obtained from the simulation results (see the dashed line in Figure 4). These two asymptotic limits can be interpolated between by the following hyperbola

$$\frac{\mu^E}{\mu^E_0}(\epsilon,Z) = \frac{\epsilon s}{2} + \frac{\tilde{\mu}^E_{low}(Z)}{2} + \frac{1}{2}\sqrt{as + \epsilon^2 s^2 - 2\epsilon s\tilde{\mu}^E_{low}(Z) + (\tilde{\mu}^E_{low}(Z))^2} \quad (27)$$

where $s = 0.67$ gives the correct high-$Z$ behavior, $\tilde{\mu}^E_{low}(Z)$ is given by eq 26, and $a$ controls the sharpness of the interpolation between the two asymptotic regimes. A value of $a = 0.4/Z^2$ gives smooth agreement with the simulation results in the crossover regime, as is shown in Figure 4.

**5.2. Comparison with Experimental Data.** In this section we quantitatively test the model against constant-field mobility data for double-stranded DNA in a range of agarose gel concentrations.[40] This procedure allows us to obtain values for the various model parameters by fitting the interpolation formula (eq 27) to experimental data for constant-field electrophoresis. Values for the Kuhn step length and the number of base pairs per Kuhn step are known to reasonable accuracy, and we use values of $b = 100$ nm and $N^{bp}_K = 300$ for these, respectively. The other required parameters are the effective charge per Kuhn step $q\xi$, the friction per Kuhn step $\zeta$, and the gel pore size $a$. The pore size specifies the number of Kuhn steps per entanglement segment via $a^2 = N_e b^2$. With values of these parameters all the reduced units in eq 19 can be converted to real quantities. Approximate values of each of these parameters are known, but they are expected to vary with temperature, gel concentration, or salt concentration. Therefore, we use these known values as a guide and make small adjustments to fit the data by Heller et al.[40] For an agarose concentration of 1% this gives values of $q\xi = 60e$, $\zeta = 1.15 \times 10^{-9}$ N s/m, and $a = 200$ nm. The comparison is shown in Figure 6, which shows electrophoretic mobility against field strength. We note that, although $\tau_e$ is not required to compute the steady-state constant-field mobility, it is still specified by these above quantities, with a value of $\tau_e = 0.047$ s. To verify this value, measurements under nonsteady conditions would be needed.

To further extend this characterization, we model the remaining agarose concentrations in the study of Heller et al.[40] The

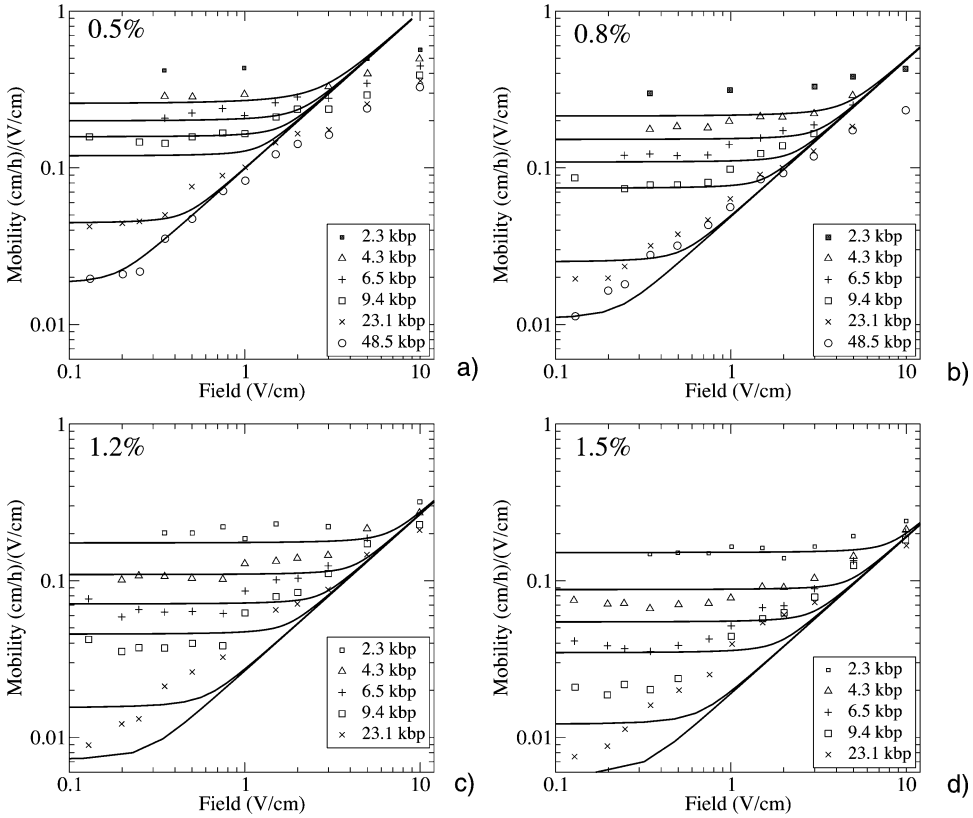


**Figure 7.** Comparison of experimental data for constant-field electrophoresis of double-stranded DNA in a range of agarose gel concentrations by Heller et al.[40] with the interpolation formula (eq 27). The concentration scaling of the model parameters is discussed in the text.

gel pore size and possibly the Kuhn step friction are expected to vary with gel concentration, $\Phi$, whereas all other parameters are fixed. By fitting the remaining data, we obtain $a \sim \Phi^{-0.5}$, which is typical for agarose gels (see for example ref 51). With this scaling of the tube diameter no scaling of the friction with gel concentration is required. The resulting comparison is shown in Figure 7. Generally, the agreement is close for well-entangled DNA at gel concentrations between 0.5% and 1.2%. There is some systematic disagreement for the shorter DNA chains at the lower gel concentrations since these systems are only marginally entangled. Agreement across all DNA lengths is weaker for the highest gel concentration of 1.5% since at this concentration $N_e = 2.67$, indicating that the tight gel limit is being approached and the model assumptions begin to break down. This data comparison demonstrates how the simulation results can be used to characterize DNA−matrix systems. The interpolation formulas (eqs 26 and 27) allow convenient fitting of constant field data, which then provides all physical parameters required by the model.

## 6. Conclusions

We have generalized an approach from rheological modeling[32] to derive a coarse-grained Brownian dynamics simulation of the motion of DNA in an entangling medium subjected to an external electric field. The influence of the field is incorporated into the strand free energy, which then influences both the monomer sliding dynamics and the renewal of entanglements at the chain ends. Also included in the modified free energy is the effect of finite chain extensibility, which is expected to be important for general time-dependent fields. Finally, we modify the chain mobility matrix so that it is consistent with the instantaneous chain configuration. The resulting algorithm provides a detailed model for DNA chain dynamics under an electric field, and it allows both bulk rheology and electrophoresis to be modeled under the same theoretical framework.

We outline a stable and efficient numerical algorithm to solve the model, which is suitable for a wide range of field conditions. Results are presented for constant field mobility, and these are shown to be consistent with both theoretically derived scaling regimes and experimental results. We provide a simple interpolation formula, describing all our constant field results, and use this formula to fit experimental data for electrophoresis of double-stranded DNA in an agarose gel matrix. The formula is able to accurately describe a range of gel concentrations using a simple scaling law for the gel pore size with concentration. This procedure allows a characterization of the DNA−gel system from constant-field data alone.

The model framework suggests that a range of further refinements are possible. It is interesting to verify if the model can also describe electrophoresis of single-stranded DNA and to compare the resulting molecular parameters with this work for double-stranded DNA. The model can also predict the degree of dispersion about the mean drift velocity, leading to a predictions of the resolution, which could also be compared with experimental results.[52] Motion of the entangling medium could be accounted for to allow modeling of linear entangling matrices in addition to cross-linked gels. This could be achieved by utilizing concepts of "constraint release'' from rheological modeling.[53,54] Hernia formation, extended chain loops protruding from the side of the tube, could be described by a generalization of the creation and destruction algorithm for entanglement junctions at the chain ends. This theoretical framework could be used to model tightly entangled chains, by taking a semiflexible expression for the strand free energy. This would allow more complete modeling of the range of gel concentrations

commonly used in electrophoresis. Again, guidance may be found in rheological theories.[55]

## Appendix A. Monomer Sliding Dynamics

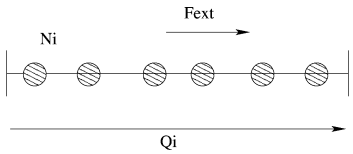


**Figure 8.** Response of the system to an external force.

In this appendix we derive a new expression for the mobility matrix, which determines the rate of monomer sliding in response to gradients in the chemical potential. We allow this quantity to fluctuate with the local chain configuration to produce an expression in which each monomer carries an equal amount of drag. We require an expression for the mobility matrix $L_{ij}$ which determines the rate of change of $N_i$ in response to differences in chemical potential. Considering a single entanglement segment in isolation, we need to find $J$ such that

$$\frac{\mathrm{d}N}{\mathrm{d}t} = J\frac{\partial F}{\partial N} \tag{28}$$

where $F$ is the strand free energy. By counting the total drag from all monomers in the segment, the rate of change of primitive path, $l$, in response to an external force is

$$\frac{\mathrm{d}l}{\mathrm{d}t} = \frac{1}{N\zeta}\frac{\partial F}{\partial l} \tag{29}$$

where $\zeta$ is the friction per monomer, and we have written the external force as the spatial derivative of a free energy, $F$. The number of monomers per unit length of primitive path is averaged over the segment to give $\mathrm{d}N = (N/Q)\mathrm{d}l$, and this expression is substituted into eq 29

$$\frac{\mathrm{d}N}{\mathrm{d}t} = \frac{1}{N\zeta}\frac{\partial F}{\partial N}\left(\frac{\mathrm{d}N}{\mathrm{d}l}\right)^2 \tag{30}$$

Comparing with eq 28 gives

$$J = \frac{N}{Q^2\zeta} = \frac{1}{k_\mathrm{B}T\tau_\mathrm{K}}\frac{\tilde{N}}{\tilde{Q}^2} \tag{31}$$

Averaging the mobility over neighboring segments allows us to define the mobility across the junction $i$, which is determined by segments $i$ and $i-1$

$$J_{i,i-1} = \frac{1}{k_\mathrm{B}T\tau_\mathrm{K}}\frac{\frac{1}{2}\tilde{N}_i + \frac{1}{2}\tilde{N}_{i-1}}{\left(\frac{1}{2}\left|\tilde{Q}_i\right| + \frac{1}{2}\left|\tilde{Q}_{i-1}\right|\right)^2} = \frac{2}{k_\mathrm{B}T\tau_\mathrm{K}}\frac{\tilde{N}_i + \tilde{N}_{i-1}}{(|\tilde{Q}_i| + |\tilde{Q}_{i-1}|)^2} \equiv \frac{1}{k_\mathrm{B}T\tau_\mathrm{K}}\tilde{J}_{i,i-1} \tag{32}$$

Fixing the values of $\tilde{N}_i$ and $\tilde{Q}_i$ at their mean equilibrium values in eq 32 will recover the mobility matrix used by ref 32. Replacing the constant mobility matrix in eq 4 with the locally varying mobility allows us to define the generalized Rouse matrix, which respects monomer conservation and chain connectivity

$$L_{ij}(\{N_i\}) = \begin{cases} J_{i,i-1} + J_{i,i+1} & \text{if } i = j \\ -J_{i,i-1} & \text{if } i-1 = j \\ -J_{i,i+1} & \text{if } i+1 = j \\ 0 & \text{otherwise} \end{cases} \tag{33}$$

The next step is to convert the Fokker−Planck equation to an equivalent Langevin equation which is achieved by the approach of ref 43. The noise term is given by

$$\sqrt{2k_\mathrm{B}T\,\mathrm{d}t}\sum_j \sigma_{ij}\,\mathrm{d}W_j \tag{34}$$

where the $\mathrm{d}W_i$ are uncorrelated Wiener increments of unit width and the matrix $\sigma_{ij}$ is related to the mobility matrix via $L_{pq} = \sum_k \sigma_{pk}\sigma_{qk}$. Thus, $\sigma$ can be determined by Cholesky decomposition to give

$$\sigma_{ij} = \begin{cases} -\sqrt{J_{i,i+1}} & \text{if } i = j \\ \sqrt{J_{i,i-1}} & \text{if } i = j+1 \end{cases} \tag{35}$$

Continuing with the algorithm, the Langevin equation becomes (by noting that $\sum_m(\partial L_{nm}/\partial N_m) = 0 \forall n$)

$$\mathrm{d}N_i(t) = -\mathrm{d}t\sum_j L_{ij}\frac{\partial F}{\partial N_j} + \sqrt{2k_\mathrm{B}T\,\mathrm{d}t}\sum_j \sigma_{ij}\,\mathrm{d}W_j \tag{36}$$

Inserting the chemical potential and the specific form of the mobility matrix (eq 33) leads to

$$\mathrm{d}N_i = \frac{\mathrm{d}t}{k_\mathrm{B}T\tau_\mathrm{K}}(\tilde{J}_{i,i-1}(\mu_{i-1} - \mu_i) + \tilde{J}_{i,i+1}(\mu_{i+1} - \mu_i)) + \sqrt{\frac{2\mathrm{d}t}{\tau_\mathrm{K}}}(\sqrt{\tilde{J}_{i,i-1}}\,\mathrm{d}W_{i-1} - \sqrt{\tilde{J}_{i,i+1}}\,\mathrm{d}W_i) \tag{37}$$

Taking an implicit time step of size $\Delta t$ and dividing by $N_\mathrm{e}$ to insert the dimensionless units (eq 19) gives

$$\tilde{N}_i(t+\Delta t) = \tilde{N}_i(t) - \frac{\Delta t}{2N_\mathrm{e}^2\tau_\mathrm{K}}[\tilde{J}_{i,i-1}(\tilde{\mu}_{i-1}(t+\Delta t) + \tilde{\mu}_{i-1}(t) - \tilde{\mu}_i(t+\Delta t) - \tilde{\mu}_i(t)) + \tilde{J}_{i,i+1}(\tilde{\mu}_{i+1}(t+\Delta t) + \tilde{\mu}_{i+1}(t) - \tilde{\mu}_i(t+\Delta t) - \tilde{\mu}_i(t))] + \sqrt{\frac{2\mathrm{d}t}{N_\mathrm{e}^2\tau_\mathrm{K}}}(\sqrt{\tilde{J}_{i,i-1}}\,\mathrm{d}W_{i-1} - \sqrt{\tilde{J}_{i,i+1}}\,\mathrm{d}W_i) \tag{38}$$

where $\tilde{\mu} = N_\mathrm{e}\mu_i/kT$ is the dimensionless chemical potential. In eq 42 $i$ runs from 1...$Z$. To ensure that the same equation holds for the dangling ends segments, we set $J_{1,0} = 0$, $J_{Z,Z+1} = 0$, which guarantees no flux into or out of the fictitious segments at $i = 0$ and $Z+1$. Since the elastic part of the free energy must be solved implicitly over the time step, we split the chemical potential into an elastic and an external field contribution.

$$\tilde{\mu}_i(\tilde{N}_i, \tilde{Q}_i, \epsilon) = \tilde{\mu}_i^{\mathrm{el}}(\tilde{N}_i, \tilde{Q}_i) + \tilde{\mu}_i^{\mathrm{ext}}(\tilde{Q}_i, \epsilon_i) \tag{39}$$

We also note that the $\tilde{Q}_i$ do not change during the monomer shuffling stage of the time step. For conciseness we define $\tilde{N}_i' = \tilde{N}_i(t+\Delta t)$ and $\tilde{\mu}_i^{\mathrm{el}} = \tilde{\mu}_i^{\mathrm{el}}(\tilde{N}_i(t+\Delta t))$. These steps allow us to separate terms depending on the unknown monomer configuration at the end of the time step, $\{\tilde{N}_i'\}$, from those that depend only on the known starting configuration, $\{\tilde{N}_i\}$. Thus

$$\tilde{N}_i' = -\frac{\Delta t}{2\tau_e}(\tilde{J}_{i,i-1} + \tilde{J}_{i,i+1})\tilde{\mu}_i^{el'} + \frac{\Delta t}{2\tau_e}[\tilde{J}_{i,i-1}\tilde{\mu}_{i-1}^{el'} + \tilde{J}_{i,i+1}\tilde{\mu}_{i+1}^{el'}] + F_i(t) \quad (40)$$

Here the $F_i$ depend only on the configuration at the start of the time step

$$F_i(t) = \tilde{N}_i - \frac{\Delta t}{\tau_e}[\tilde{J}_{i,i-1}(\tilde{\mu}_i^{ext} - \tilde{\mu}_{i-1}^{ext}) + \tilde{J}_{i,i+1}(\tilde{\mu}_i^{ext} - \tilde{\mu}_{i+1}^{ext})] - \frac{\Delta t}{2\tau_e}[\tilde{J}_{i,i-1}(\tilde{\mu}_i^{el} - \tilde{\mu}_{i-1}^{el}) + \tilde{J}_{i,i+1}(\tilde{\mu}_i^{el} - \tilde{\mu}_{i+1}^{el})] + \sqrt{\frac{2\Delta t}{\tau_e}}(\sqrt{\tilde{J}_{i,i-1}}\, dW_{i-1} - \sqrt{\tilde{J}_{i,i+1}}\, dW_i) \quad (41)$$

and the difference in field potential between neighboring segments is

$$\tilde{\mu}_i^{ext} - \tilde{\mu}_{i-1}^{ext} = -\epsilon\left[\frac{1}{2}\tilde{Q}_i \cos\theta_i + \frac{1}{2}\tilde{Q}_{i-1}\cos\theta_{i-1}\right] \quad (42)$$

The desired form for the elastic part of the free energy can now be substituted in to yield the system of nonlinear equations that is to be solved. If the Gaussian form is used, then the iterative scheme used by Schieber et al.,[32] which involves solving a cubic equation for each segment at each iteration step, will still work in this case. For the finitely extensible form of the free energy we solve the entire system by using a standard multidimensional Newton root-finding approach, which utilizes a line search and backtracking algorithm (see section 9.7 in ref 56).

### Appendix B. Creation and Destruction Probabilities with Electric Field

First we consider a Gaussian chain in an external field. Substituting eqs 11, 12, and 9 into the detailed balance expression (eq 8) gives

$$W^c(\tilde{\mathbf{Q}}_s,\tilde{N}_s,\tilde{N}_E) = \frac{1}{\tau_e}\sqrt{\frac{3}{\tilde{N}_E}}\left(\frac{3}{2\pi\tilde{N}_s}\right)^{3/2}\exp\left[-\frac{3\tilde{Q}_s^{\,2}}{2\tilde{N}_s} + \epsilon\left(\tilde{N}_E - \frac{1}{2}\tilde{N}_s\right)\tilde{Q}_s\cos\theta_s\right] d\tilde{\mathbf{Q}}_s^{\,3}\, d\tilde{N}_s \quad (43)$$

Integrating overall values of $\tilde{\mathbf{Q}}_s$ gives

$$p(\tilde{N}_s, \tilde{N}_E) = \frac{1}{\tau_e}\sqrt{\frac{3}{\tilde{N}_E}}\exp\left[\frac{\epsilon^2}{24}\tilde{N}_s(\tilde{N}_s - 2\tilde{N}_E)^2\right] d\tilde{N}_s \quad (44)$$

Continuing with the integration over $\tilde{N}_s = 0...\tilde{N}_E$ yields the probability per unit time of entanglement creation, $w^c(\tilde{N}_E)$.

$$w^c(\tilde{N}_E) = \frac{1}{\tau_e}\sqrt{\frac{3}{\tilde{N}_E}}\left(\frac{24}{\epsilon^2}\right)^{1/3}\mathrm{CubicExpInt}\left[\left(\frac{\epsilon^2}{24}\right)^{1/3}\tilde{N}_E\right] \quad (45)$$

where

$$\mathrm{CubicExpInt}(x) = \int_0^x \exp(t^3 - 4t^2x + 4tx^2)\, dt \quad (46)$$

We derive an efficient and accurate method of approximating this integral for all $x$ in Appendix B.1. An expression for the conditional probability, $p(\tilde{N}_s|\tilde{N}_E)$, is obtained by dividing eq 44 by eq 45.

$$p(\tilde{N}_s|\tilde{N}_E) = \left(\frac{\epsilon^2}{24}\right)^{1/3}\frac{\exp[(\epsilon^2/24)\tilde{N}_s(\tilde{N}_s - 2\tilde{N}_E)^2]}{\mathrm{CubicExpInt}[(\epsilon^2/24)^{1/3}\tilde{N}_E]}\, d\tilde{N}_s \quad (47)$$

This distribution defines the number of monomers to be placed inside a newly created segment. Random numbers with this distribution can be generated using the rejection method[56] by taking, for the trial function, the maximum value of $p(\tilde{N}_s|\tilde{N}_E)$ on $[0, \tilde{N}_E]$. For moderate values of the field the shape of $p(\tilde{N}_s|\tilde{N}_E)$ is smooth enough that the rejection method is efficient. For larger fields the distribution in eq 47 tends to a Gaussian distribution, and $\tilde{N}_s$ can generated by exploiting this.

Given the number of monomers in the new strand, $\tilde{N}_s$, next we generate the orientation vector of the strand, $\tilde{\mathbf{Q}}_s$, consistently with the value of $\tilde{N}_s$. The appropriate conditional probability is

$$p(\tilde{\mathbf{Q}}_s|\tilde{N}_s, \tilde{N}_E) = \frac{p(\tilde{\mathbf{Q}}_s,\tilde{N}_s,\tilde{N}_E)}{p(\tilde{N}_s,\tilde{N}_E)} = \tilde{Q}_s^{\,2}\left(\frac{3}{2\pi\tilde{N}_s}\right)^{3/2}\exp\left[-\frac{3\tilde{Q}_s^{\,2}}{2\tilde{N}_s} + \epsilon\left(\tilde{N}_E - \frac{1}{2}\tilde{N}_s\right)\tilde{Q}_s\cos\theta - \frac{\epsilon^2}{24}\tilde{N}_s(\tilde{N}_s - 2\tilde{N}_E)^2\right] d\tilde{Q}_s\sin\theta\, d\theta\, d\phi \quad (48)$$

which gives the usual Gaussian distribution when $\epsilon \to 0$. Clearly, $\phi$ is distributed evenly between $0...2\pi$. Integrating over both angles gives the distribution of entanglement lengths

$$p(\tilde{Q}_s|\tilde{N}_s,\tilde{N}_E) = A\tilde{Q}_s\exp\left[-\frac{3\tilde{Q}_s^{\,2}}{2\tilde{N}_s}\right]\sinh\left(\epsilon\left(\tilde{N}_E - \frac{1}{2}\tilde{N}_s\right)\tilde{Q}_s\right) \quad (49)$$

where the normalization constant, $A$, is

$$A = \frac{4\pi}{\epsilon\left(\tilde{N}_E - \frac{1}{2}\tilde{N}_s\right)}\left(\frac{3}{2\pi\tilde{N}_s}\right)^{3/2}\exp\left[-\frac{\epsilon^2}{6}\tilde{N}_s\left(\tilde{N}_E - \frac{1}{2}\tilde{N}_s\right)^2\right] \quad (50)$$

Values for $\tilde{Q}_s$ are generated from eq 49 using a similar strategy to that used to generate $\tilde{N}_s$. Finally, we generate the angle of the new strand with the field, $\theta$, from

$$p(\theta|\tilde{Q}_s,\tilde{N}_s,\tilde{N}_E) = \frac{\epsilon\left(\tilde{N}_E - \frac{1}{2}\tilde{N}_s\right)\tilde{Q}_s}{2\sinh\left(\epsilon\left(\tilde{N}_E - \frac{1}{2}\tilde{N}_s\right)\tilde{Q}_s\right)}\times \exp\left[\epsilon\left(\tilde{N}_E - \frac{1}{2}\tilde{N}_s\right)\tilde{Q}_s\cos\theta\right]\sin\theta\, d\theta \quad (51)$$

The angular distribution is Boltzmann weighted in the field potential of the new strand, similar to previous theories.[33] However, in these earlier approaches the number of monomers used in the Boltzmann weighting was arbitrarily set at the average number per segment in equilibrium, $N_e$, whereas with this algorithm we generate the number of monomers and length of the new segment from a stochastic algorithm that is determined self-consistently from the chain free energy. The distribution for $\cos\theta$ can be integrated and inverted to give an analytic selection rule

$$\cos\theta = \frac{1}{\epsilon\tilde{Q}_sX}\ln[\exp(-\epsilon X\tilde{Q}_s) + 2\xi\sinh(\epsilon X\tilde{Q}_s)] \quad (52)$$

where $\xi$ is chosen randomly from an even distribution between $0...1$ and $X = (\tilde{N}_E - {}^1/_2\tilde{N}_s)$.

**Table 1. Values for Quotient Approximation of $G(x)$**

| | $k$ | | | | |
|---|---|---|---|---|---|
| | 1 | 2 | 3 | 4 | 5 |
| $a_k$ | N/A | N/A | N/A | 1.564 | −1.577 |
| $b_k$ | 2.065 | −2.111 | 0.317 | 2.228 | −1.692 |

The above derivation provides expressions for the probability of entanglement creation along with distributions for the details of the new segment. We test $w^c(\tilde{N}_E)$ at each simulation time step and, if the test is positive, generate a new segment with $\tilde{\mathbf{Q}}_s$ and $\tilde{N}_s$ given by the above conditional probability distributions. The procedure can be repeated using the finitely extensible free energy to produce an equivalent entanglement renewal algorithm. See Appendix B.2 for this derivation.

**B.1. Cubic Exponential Integral Evaluation.** In this appendix we seek an efficient method to evaluate the numerical integral in eq 46. We note that the integral can be written as

$$\mathrm{CubicExpInt}(x) = \int_0^x \exp[f_x(t)]\,\mathrm{d}t \tag{53}$$

where $f_x(t) = t^3 - 4t^2x + 4tx^2$. For large $x$, most of the area under the integrand, in the range of integration, is focused around the maximum of $f_x(t)$ at $t = 2x/3$, and the integrand is approximately Gaussian in this region. We may take a second-order expansion of $f_x(t)$ around this maximum to obtain an approximate Gaussian form for the integrand.

$$\mathrm{CubicExpInt}(x) \approx \exp\left(\frac{32x^3}{27}\right)\int_{-\infty}^{\infty}\exp\left(-2x\left(t-\frac{2x}{3}\right)^2\right)\mathrm{d}t \qquad \text{for } x \gg 1$$

$$= \exp\left(\frac{32x^3}{27}\right)\sqrt{\frac{\pi}{2x}} \tag{54}$$

To account for all $x$, we write the integral as

$$\mathrm{CubicExpInt}(x) = \sqrt{\frac{\pi}{2x}}\exp\left(\frac{32x^3}{27}\right)G(x) \tag{55}$$

where

$$G(x) = \sqrt{\frac{2x}{\pi}}\int_0^x \exp(t^3 - 4t^2x + 4tx^2 - 32x^3/27)\,\mathrm{d}t \tag{56}$$

The function $G(x)$ is relatively smooth, and $G(x) \approx \sqrt{2/\pi}x^{3/2}$ for $x \ll 1$ and $G(x) \to 1$ as $x \to \infty$. Thus, it can be approximated by a quotient of the form

$$G(x) \approx \frac{\sqrt{(2/\pi)}x^{3/2} + \sum_{k=1}^{N-1} a_k x^{k/2} + x^{N/2}}{1 + \sum_{k=1}^{N-1} b_k x^{k/2} + x^{N/2}} \tag{57}$$

The $a_k$ and $b_k$ are found by fitting eq 57 to values of $G(x)$ produced by numerical integration. Taking $N = 6$ produces agreement within 1% $\forall x$, and coefficients for this approximation are given in Table 1.

**B.2. Entanglement Renewal for the Finitely Extensible Free Energy.** In this appendix we rederive the entanglement renewal algorithm using the modified finitely extensible free energy. Proceeding as in section B, we substitute the desired free energy expression into the detailed balance expression (eq 8). Switching to spherical polar coordinates gives

$$W^c(\tilde{\mathbf{Q}}_s,\tilde{N}_s,\tilde{N}_E) = \frac{1}{\tau_e}\sqrt{\frac{3}{\tilde{N}_E}}\left(\frac{3}{2\pi\tilde{N}_s}\right)^{3/2}\exp\left[-\frac{\tilde{Q}_s^{\,2}}{2\tilde{N}_s} + \epsilon\left(\tilde{N}_E - \frac{1}{2}\tilde{N}_s\right)\tilde{Q}_s\cos\theta_s\right]\left(1-\left(\frac{\tilde{Q}_s}{\sqrt{N_e}\tilde{N}_s}\right)^2\right)^{N_e\tilde{N}_s}\mathrm{d}\tilde{\mathbf{Q}}_s^{\,3}\,\mathrm{d}\tilde{N}_s \tag{58}$$

We define $\lambda = \sqrt{N_e}$ and $X = \epsilon(\tilde{N}_E - \tilde{N}_s/2)$ and integrate $W^c$ over both the azimuthal and polar angle to give

$$p(\tilde{Q}_s,\tilde{N}_s,\tilde{N}_E) = \frac{2\pi}{\tau_e}\sqrt{\frac{3}{\tilde{N}_E}}\left(\frac{3}{2\pi\tilde{N}_s}\right)^{3/2}\frac{2}{X}\sinh(\tilde{Q}_sX)\exp\left(-\frac{\tilde{Q}_s^{\,2}}{2\tilde{N}_s}\right)\left(1-\frac{\tilde{Q}_s^{\,2}}{\lambda_s^2\tilde{N}_s^{\,2}}\right)^{\lambda\tilde{N}_s}\tilde{Q}_s\,\mathrm{d}\tilde{Q}_s\,\mathrm{d}\tilde{N}_s \tag{59}$$

where $p(\tilde{Q}_s,\tilde{N}_s,\tilde{N}_E)$ is the probability per unit time of creating, from an initial dangling end of $\tilde{N}_E$ monomers, a new segment of length $\tilde{Q}_s$, containing $\tilde{N}_s$ monomers. The integral over $\tilde{Q}_s$ cannot be performed analytically, however, substituting in the power series expansion of $\sinh(x) = \sum_{i\ \mathrm{odd}}(x^i/i!)$ allows us to proceed

$$p(\tilde{N}_s,\tilde{N}_E) = \frac{2\pi}{\tau_e}\sqrt{\frac{3}{\tilde{N}_E}}\left(\frac{3}{2\pi\tilde{N}_s}\right)^{3/2}2\sum_{i\ \mathrm{odd}}X^{i-1}\frac{1}{i!}\int_0^{\lambda}\tilde{N}\tilde{Q}_s^{\,i}\exp\left(-\frac{\tilde{Q}_s^{\,2}}{2\tilde{N}_s}\right)\left(1-\frac{\tilde{Q}_s^{\,2}}{\lambda_s^2\tilde{N}_s^{\,2}}\right)^{\lambda\tilde{N}}\tilde{Q}_s\,\mathrm{d}\tilde{Q}_s\,\mathrm{d}\tilde{N}_s \tag{60}$$

The integral over $\tilde{Q}_s$ is analytic for all values of $i$

$$p(\tilde{N}_s,\tilde{N}_E) = \frac{2\pi}{\tau_e}\sqrt{\frac{3}{\tilde{N}_E}}\left(\frac{3}{2\pi\tilde{N}_s}\right)^{3/2}\sum_{i\ \mathrm{odd}}X^{i-1}\frac{\Gamma(1+i/2)}{i!}\tilde{N}_s^{\,3+i}\lambda^{4+i}\Gamma(\tilde{N}_s\lambda^2)\,{}_1F_1\left(1+\frac{i}{2},2+\frac{i}{2}+\tilde{N}_s\lambda^2,-\frac{\tilde{N}_s\lambda^2}{2}\right)\mathrm{d}\tilde{N}_s \tag{61}$$

where ${}_1F_1(a,b,z)$ is the confluent hypergeometric function of the first kind. Defining $\upsilon = \lambda^2\tilde{N}_s$, $x = \tilde{N}_E\lambda^2$, and $i = 2k + 1$ allows

$$p(\tilde{N}_s,\tilde{N}_E) = \frac{2\pi}{\tau_e}\sqrt{\frac{3}{\tilde{N}_E}}\left(\frac{3}{2\pi}\right)^{3/2}\sum_{k=0}^{\infty}\frac{\Gamma(3/2+k)}{(2k+1)!}\left[\frac{\epsilon\upsilon(x-\upsilon/2)}{\lambda^3}\right]^{2k}\Gamma(\upsilon)\upsilon^{5/2}\,{}_1F_1\left(\frac{3}{2}+k,\frac{5}{2}+k+\upsilon,-\frac{\upsilon}{2}\right)\mathrm{d}\tilde{N}_s \tag{62}$$

One can show that the radius of convergence of this series is infinite for all $\upsilon > 0$ by first noting that ${}_1F_1({}^3/_2 + k, {}^5/_2 + k + \upsilon, -{}^{\upsilon}/_2)$ asymptotically tends to $\exp(-\upsilon/2)$ as $k \to \infty$ and then applying the Cauchy ratio test. Furthermore, our evaluations of eq 62 show that $p(\tilde{N}_s,\tilde{N}_E)$ is relatively smooth and requires only a small number of terms for the sum to converge, provided both $\epsilon, \lambda \lesssim 30$. Thus, numerical evaluation of

$$w^c(\tilde{N}_E) = \int_0^{\tilde{N}_E} p(\tilde{N}_s,\tilde{N}_E)\,\mathrm{d}\tilde{N}_s \tag{63}$$

is fairly inexpensively. We use the rejection method to generate $\tilde{N}_s$ given $\tilde{N}_E$, picking the trial function to be a constant function taking the value of the maximum of eq 62. This maximum is

found numerically using the golden search algorithm [see section 10.1 of ref 56]. A single evaluation of $w^c(\tilde{N}_E)$ provides the normalization constant.

For the high field limit, where $\epsilon > \lambda$ and $\lambda \lesssim 30$, each of the integrands can be approximated by a Gaussian function in a similar approximation method to that used in Appendix B.1. This obviates the need evaluate the problematically large normalization functions since a Gaussian distribution can be readily generated once the mean and variance are known.

## References and Notes


(1) Burns, M. A. *Science* **2002**, *296*, 1818.
(2) Slater, G. W.; Desrulsseaux, C.; Hubert, S. J.; Mercier, J. F.; Labrie, J.; Boileau, J.; Tessier, F.; Pepin, M. P. *Electrophoresis* **2000**, *21*, 3873.
(3) Burke, D. T.; Carle, G. F.; Olson, M. V. *Science* **1987**, *236*, 806.
(4) Langer-Safer, P. R.; Levine, M.; Ward, D. C. *Proc. Natl. Acad. Sci. U.S.A.* **1982**, *79*, 4381.
(5) Carle, G. F.; Frank, M.; Olson, M. V. *Science* **1986**, *232*, 65.
(6) Gurrieri, S.; Smith, S. B.; Wells, K. S.; Johnson, I. D.; Bustamante, C. *Nucleic Acids Res.* **1996**, *24*, 4759.
(7) Gardiner, K. *Anal. Chem.* **1991**, *63*, 658.
(8) Oana, H.; Ueda, M.; Washizu, M. *Biochem. Biophys. Res. Commun.* **1999**, *265*, 140.
(9) Jing, J. P.; Reed, J.; Huang, J.; Hu, X. H.; Clarke, V.; Edington, J.; Housman, D.; Anantharaman, T. S.; Huff, E. J.; Mishra, B.; Porter, B.; Shenker, A.; Wolfson, E.; Hiort, C.; Kantor, R.; Aston, C.; Schwartz, D. C. *Proc. Natl. Acad. Sci. U.S.A.* **1998**, *95*, 8046.
(10) Schwartz, D. C.; Li, X. J.; Hernandez, L. I.; Ramnarain, S. P.; Huff, E. J.; Wang, Y. K. *Science* **1993**, *262*, 110.
(11) Ueda, M.; Yoshikawa, K.; Doi, M. *Polym. J.* **1997**, *29*, 1040.
(12) Ueda, M. *J. Biochem. Biophys. Methods* **1999**, *41*, 153.
(13) Kaji, N.; Ueda, M.; Baba, Y. *Biophys. J.* **2002**, *82*, 335.
(14) Burns, M. A.; Johnson, B. N.; Brahmasandra, S. N.; Handique, K.; Webster, J. R.; Krishnan, M.; Sammarco, T. S.; Man, P. M.; Jones, D.; Heldsinger, D.; Mastrangelo, C. H.; Burke, D. T. *Science* **1998**, *282*, 484.
(15) Namasivayam, V.; Larson, R. G.; Burke, D. T.; Burns, M. A. *Anal. Chem.* **2002**, *74*, 3378.
(16) Olvera de la Cruz, M.; Deutsch, J. M.; Edwards, S. F. *Phys. Rev. A* **1986**, *33*, 2047.
(17) Deutsch, J. M. *Phys. Rev. Lett.* **1987**, *59*, 1255.
(18) Deutsch, J. M. *Science* **1988**, *240*, 922.
(19) Doi, M.; Edwards, S. F. *The Theory of Polymer Dynamics*; Oxford University Press: Oxford, 1986.
(20) McLeish, T. C. B. *Adv. Phys.* **2002**, *51*, 1379.
(21) Graham, R. S.; Likhtman, A. E.; McLeish, T. C. B.; Milner, S. T. *J. Rheol.* **2003**, *47*, 1171.
(22) Likhtman, A. E. *Macromolecules* **2005**, *38*, 6128.
(23) Slater, G. W.; Noolandi, J. *Phys. Rev. Lett.* **1985**, *55*, 1579.
(24) Duke, T.; Viovy, J. L.; Semenov, A. N. *Biopolymers* **1994**, *34*, 239.
(25) Viovy, J. L. *Rev. Mod. Phys.* ***2000***, *72*, 813.
(26) Noolandi, J.; Slater, G. W.; Lim, H. A.; Viovy, J. L. *Science* **1989**, *243*, 1456.
(27) Heo, Y.; Larson, R. G. *J. Rheol.* **2005**, *49*, 1117.
(28) Teixeira, R. E.; Babcock, H. P.; Shaqfeh, E. S. G.; Chu, S. *Macromolecules* **2005**, *38*, 581.
(29) Teixeira, R.; Shaqfeh, E.; Chu, S. In *The Society of Rheology: 77th Annual Meeting Program and Abstracts*, 2005.
(30) Masubuchi, Y.; Takimoto, J. I.; Koyama, K.; Ianniruberto, G.; Marrucci, G.; Greco, F. *J. Chem. Phys.* **2001**, *115*, 4387.
(31) Tasaki, H.; Takimoto, J.; Doi, M. *Comput. Phys. Commun.* **2001**, *142*, 136.
(32) Schieber, J. D.; Neergaard, J.; Gupta, S. *J. Rheol.* **2003**, *47*, 213.
(33) Zimm, B. H. *J. Chem. Phys.* **1991**, *94*, 2187.
(34) Zimm, B. H. *Phys. Rev. Lett.* **1988**, *61*, 2965.
(35) Higgins, J. S.; Benoît, H. C. *Polymer and Neutron Scattering*; Clarendon Press: Oxford, 1994.
(36) Milner, S. T.; McLeish, T. C. B.; Likhtman, A. E. *J. Rheol.* **2001**, *45*, 539.
(37) Shanbhag, S.; Larson, R. G.; Takimoto, J.; Doi, M. *Phys. Rev. Lett.* **2001**, *87*, 195502.
(38) Duke, T. A. J.; Semenov, A. N.; Viovy, J. L. *Phys. Rev. Lett.* **1992**, *69*, 3260.
(39) Duke, T. A. J.; Viovy, J. L. *J. Chem. Phys.* **1992**, *96*, 8552.
(40) Heller, C.; Duke, T.; Viovy, J. L. *Biopolymers* **1994**, *34*, 249.
(41) Hutson, M. S.; Holzwarth, G.; Duke, T.; Viovy, J. L. *Biopolymers* **1995**, *35*, 297.
(42) Schieber, J. D. *J. Chem. Phys.* **2003**, *118*, 5162.
(43) Ermak, D.; McCammon, J. A. *J. Chem. Phys.* **1978**, *69*, 1352.
(44) Flory, P. J. *Statistical Mechanics of Chain Molecules*; John Wiley and Sons: New York, 1969.
(45) Cohen, A. *Rheol. Acta* **1991**, *30*, 270.
(46) Hur, J. S.; Shaqfeh, E. S. G.; Larson, R. G. *J. Rheol.* **2000**, *44*, 713.
(47) Chasovskikh, V. V.; Frumin, L. L.; Peltek, S. E.; Zilberstein, G. V. *Phys. Chem. Chem. Phys.* **2002**, *4*, 2691.
(48) Slater, G. W.; Drouin, G. *Electrophoresis* **1992**, *13*, 574.
(49) Pluen, A.; Tinland, B.; Sturm, J.; Weill, G. *Electrophoresis* **1998**, *19*, 1548.
(50) Semenov, A. N.; Duke, T. A. J.; Viovy, J. L. *Phys. Rev. E* **1995**, *51*, 1520.
(51) Tinland, B.; Pernodet, N.; Weill, G. *Electrophoresis* **1996**, *17*, 1046.
(52) Brahmasandra, S. N.; Burke, D. T.; Mastrangelo, C. H.; Burns, M. A. *Electrophoresis* **2001**, *22*, 1046.
(53) Rubinstein, M.; Colby, R. H. *J. Chem. Phys.* **1988**, *89*, 5291.
(54) Viovy, J. L.; Rubinstein, M.; Colby, R. H. *Macromolecules* **1991**, *24*, 3587.
(55) Morse, D. C. *Macromolecules* **1998**, *31*, 7030.
(56) Press, W. H.; Flannery, B. P.; Teukolsky, S. A.; Vetterling, W. T. *Numerical Recipes in C: The Art of Scientific Computing*; Cambridge University Press: Cambridge, 1992.


MA061912+